

Yuanyuan Li · William L. Roberts · Michael S. Brown
James R. Gord

Acoustic damping rate measurements in binary mixtures of atomic species via transient-grating spectroscopy

Received: 28 February 2005 / Revised: 6 May 2005 / Accepted: 9 May 2005 / Published online: 14 June 2005
© Springer-Verlag 2005

Abstract The objective of this work is to investigate the ability of transient-grating spectroscopy (TGS) to measure accurately the acoustic damping rate by analyzing the temporal behavior of laser-induced gratings. Experiments are performed in a binary gaseous mixture, with a trace amount of NO₂, as a function of both composition and pressure. Measured and theoretically calculated acoustic damping rates are compared using both a classical model and a more comprehensive model that included additional diffusive mechanisms. The TGS technique demonstrated here provides a nearly instantaneous measurement with reasonably high spatial resolution. The experimental data agree well with theoretical predictions.

Keywords Transient-grating spectroscopy · Acoustic dissipation · Optical diagnostics · Laser-induced thermal acoustics

1 Introduction

The transient-grating spectroscopy (TGS) or laser-induced thermal-acoustics (LITA) signal is generated by the first-order Bragg scattering of a probe beam from a laser-induced dynamic grating. The temporal behavior of the generated signal provides information on the local

speed of sound and transport properties, namely, viscosity and thermal conductivity. Laser-induced grating techniques have been utilized to explore time-dependent phenomena (initially) in liquids and solids and (more recently) in gases (Eichler et al. 1986; Govoni et al. 1993). Recent efforts include continuing development of the TGS technique for thermometry and velocimetry because of its relative simplicity and because it is a frequency-based rather than an amplitude-based technique, making it attractive for application in practical hardware (Brown and Roberts 1999). Furthermore, the amplitude of the signal scales quadratically with density—a definite advantage in high-pressure combustion environments, where many other laser-based diagnostics encounter various difficulties related to the rapid energy transfer of excited electronic states and spectral line broadening.

The decay rate of the TGS signal magnitude is a function of both thermal diffusion and acoustic damping. Through the use of an unfocused beam setup, acoustic damping rates from various pure gaseous species were investigated previously (Li et al. 2002). The experimental results from these pure species were compared to the classical acoustic damping rate, which models the effect of both thermal and viscous dissipation. The classical acoustic damping rate theory accurately predicts the decay rates in pure atomic species. However, the measured acoustic damping rates for diatomic and polyatomic gases are always higher than the calculated classical acoustic damping rates. The reason for this is that the classical theory does not account for the energy transfer from the translational mode to vibrational and/or rotational modes, and these additional energy transfer mechanisms lead to a faster decay rate. Analysis shows that the acoustic damping rate increases with molecular structure, pressure, and acoustic frequency.

The attenuation of acoustic waves in binary monatomic gas mixtures was successfully measured in the 1950s and 1960s (Holmes and Tempest 1960; Law et al. 1966; Prangma et al. 1970). The experimental results

Y. Li · W. L. Roberts (✉)
Department of Mechanical and Aerospace Engineering,
North Carolina State University,
Raleigh, NC 27695-7910, USA
E-mail: wlrobert@eos.ncsu.edu
Tel.: +1-919-5155294
Fax: +1-919-5157968

M. S. Brown
Innovative Scientific Solutions Inc, 2766 Indian Ripple Road,
Dayton, OH 45440-3638, USA

J. R. Gord
Air Force Research Laboratory, Propulsion Directorate,
Wright-Patterson Air Force Base, OH 45433-7251, USA

agreed well with Kohler's theory of absorption (Kohler 1941, 1949), where the total absorption is due to viscous dissipation, heat conduction, mass diffusion, and thermal diffusion. In most of the conventional acoustic studies (Herzfeld and Litovitz 1959), external sound sources are used to generate traveling sound waves that are detected by receivers after propagation over fixed distances. The absorption coefficient, α , is then determined by comparing the sound wave intensities at different locations along the propagation path. Accurate distance-based measurements often require a propagation path on the order of 1 m (Law et al. 1966), making them difficult in confined geometries. Because of the time-consuming and space-based nature of this traditional measurement technique, it can be applied only to homogeneous static environments.

In the present paper, we report an investigation of acoustic damping rates of helium–argon (He–Ar) mixtures in a pressurized environment (up to 7.4 atm) using TGS. In executing the TGS technique, an instantaneous ultrasonic sound wave is generated by a pair of crossed laser pulses. The intensity of the dynamic sound wave that is decaying with time in the probe volume is “read out” by a continuous-wave laser beam. Analysis of the resulting signal beam reveals the sound wave attenuation. The non-intrusive TGS technique is able to measure the acoustic wave attenuation at a single point, making it useful in environments with spatial gradients. The lifetime of the TGS signal is on the order of 1 μ s in the present study; therefore, the technique yields useful data in turbulent environments. The TGS signal intensity grows quadratically with density, making it very attractive for pressurized environments. Since the sound wave is generated by crossed laser pulses, the acoustic wavelength is determined by the optical wavelength and beam-crossing angle. This typically produces acoustic wavelengths on the order of a few tens of microns, which restricts TGS measurements to the ultrasonic regime. Because it is very difficult to generate detectable TGS signals in pure helium, in the present study, a trace amount of NO₂ was added to aid signal generation.

1.1 Transient-grating spectroscopy

The principal of the TGS technique has been discussed in detail elsewhere (Eichler et al. 1986; Cummings et al. 1995; Paul et al. 1995; Brown and Roberts 1999). Here, only a brief description is given to illustrate the fundamentals of the technique. An optical intensity grating can be generated when two laser beams with parallel, linear polarization are spatially and temporally overlapped. The grating spacing, Λ , is given by:

$$\Lambda = \frac{\lambda}{2 \sin(\frac{\theta}{2})} \quad (1)$$

The wavelength of the grating-inducing beams is given by λ , while the full angle between the beams is

denoted by θ . Through various processes, e.g., electrostriction and thermalization, the light intensity grating produces a modulation in the local density, $\Delta\rho$, and, therefore, in the local index of refraction, Δn . The hydrodynamic response of the gas to the local density disturbance is the production of two counter-propagating acoustic waves and a non-propagating, but diffusing, entropy or thermal wave. The alternating constructive and destructive interference of the two counter-propagating waves produces a standing sound wave. Therefore, the local index-of-refraction oscillates at a frequency (the Brillouin frequency) that is determined solely by the grating spacing and the local speed of sound. In the experiments presented here, the pulsed pump beams that form the grating (ideally, delta functions in time), have a pulse width of ~ 10 ns. After the grating-inducing pulses have passed through the sample volume, the grating structures themselves will be washed out in time because of the dissipation of both the acoustic and the thermal waves. If a long-pulse or continuous-wave probe beam illuminates the grating under the Bragg-scattering (coherent-scattering) condition, the optical grating can be efficiently read out. The Bragg-scattered signal is detected with a photomultiplier tube and stored on a fast-sampling oscilloscope. The TGS signal appears as an exponentially damped oscillation. For excitation by an infinitely short laser pulse at $t=0$, the signal will be given approximately for $t>0$ as (Brown and Roberts 1999):

$$I_{\text{signal}}(t) = \eta \{ A \exp(-D_{\text{th}} q^2 t) + B \exp(-\Gamma q^2 t) \cos(mc_s q t + \phi) \}^2 \quad (2)$$

In the above, D_{th} denotes the thermal diffusivity, Γ the acoustic damping coefficient, c_s the speed of sound, and $m=1$ or 2 for thermal or electrostrictive signals, respectively. The grating wave vector q is defined as $q=2\pi/\Lambda$. The expression in the curly brackets fully describes the time dependence of the TGS signal. The prefactor, η , denotes amplitude scaling factors. It is proportional to the product of the squares of the density and the optical absorption coefficient, $\rho_0^2 \alpha_{\text{opt}}^2$, for signal generation through thermalization. For signal generation via electrostriction, η is proportional to the product of the squares of the density and the electrostriction coefficient, $\rho_0^2 \epsilon^2$. The coefficients A and B , and the phase angle ϕ are used as fitting parameters. It should be noted that Eq. 2 presumes an infinitely fast thermalization rate, a pump laser with an infinitely narrow pulse width, and pump and probe beams with plane wave fronts of infinite extent. In Eq. 2, the exponential factor of the second term represents the absorption of the acoustic wave intensity.

The frequency of the standing acoustic wave is solely determined by the ratio of the local sound speed and the grating spacing, c_s/Λ . The frequency of the TGS signal generated through electrostriction is equal to twice this ratio. During electrostriction, the local fluid experiences compression and rarefaction during every grating peri-

od; thus, the density variation, $\Delta\rho$, as well as the index-of-refraction, Δn , changes its sign during every period. As a consequence, the reflectance of the fluid has two peaks within every period. If the grating is generated by thermalization, the fluid experiences rarefaction only. The reflectance reaches its maximum when $\Delta\rho$ reaches its minimum. Therefore, the frequency of the TGS signal generated through thermalization is the same as that of the standing acoustic wave.

1.2 Acoustic damping rate Γ

The attenuation of acoustic waves can be caused by various kinetic processes in the fluid, including the transport of heat and momentum, vibrational and rotational relaxation, and chemical or structural changes on a molecular scale (Trusler 1991). For single-atom species, the acoustic wave attenuation is caused by friction and heat conduction, which can be described by the classical acoustic damping rate. For multi-atom species with internal structures, translational energy is transferred to vibrational/rotational energy along with the redistribution of translational momentum. Hence, the acoustic waves attenuate faster than what is predicted by the classical acoustic damping rate. This phenomenon has been observed in earlier TGS experimental investigations (Li et al. 2002). For mixtures of atomic species, the density and temperature gradients caused by the sound waves will also generate species concentration gradients that will be damped by diffusion. Therefore, the effect of mass diffusion should be included in the description of acoustic wave absorption.

In previous traditional studies of acoustic wave attenuation in binary monatomic mixtures, the measured absorption coefficient, α , was defined by the decay of the sound wave amplitude with distance as $\exp(-\alpha z)$. This definition of absorption is well suited for explaining the results of measurements of acoustic amplitude at various distances from a transmitter. In TGS measurements, the acoustic damping rate, Γ , gives the sound wave attenuation in time, as defined in Eq. 2. The absorption coefficient, α , and the acoustic damping rate, Γ , are related in a simple way as follows:

$$\Gamma = \frac{\alpha c_s}{q^2} \quad (3)$$

In the classical view, the energy of the sound wave is dissipated as a result of both friction and heat conduction; therefore, the damping rate of the amplitude of an acoustic wave is a function of the transport properties of viscosity and thermal conductivity. The classical acoustic damping coefficient in a gas can be expressed as (Trusler 1991):

$$\Gamma_c = \frac{1}{2\rho_0} \left[\frac{4}{3}\mu + (\gamma - 1)\frac{\kappa}{c_p} \right] \quad (4)$$

where μ is the dynamic viscosity (with both shear and bulk contributions), κ the thermal conductivity, c_p the heat capacity at constant pressure, γ the ratio of specific heats, and ρ_0 is the gas density.

For a mixture of two monatomic gases, the additional acoustic wave absorption arising from diffusion between two species can be evaluated as (Trusler 1991):

$$\Gamma_d = \frac{1}{2}\gamma x_1 x_2 D \left[\frac{M_2 - M_1}{M} + \frac{\gamma - 1}{\gamma x_1 x_2} K_T \right]^2 \quad (5)$$

where M_1 and M_2 are the molecular weights of the two component gases, x_1 and x_2 their mole fractions in the mixture, $M = x_1 M_1 + x_2 M_2$, D denotes the binary mass diffusion coefficient, and K_T is the thermal diffusion ratio—which, in turn, is a function of temperature, concentration, and molecular weight. For single atomic species, $M_1 = M_2$, the thermal diffusion ratio is zero, and Eq. 5 is identically zero; thus, only viscous dissipation and heat conduction contribute to acoustic wave attenuation.

The total acoustic damping rate in an He–Ar mixture is the sum of the classical acoustic damping rate, Γ_c , and the diffusive acoustic damping rate, Γ_d . To estimate the acoustic damping rate, the parameters in Eqs. 4 and 5—namely, density ρ_0 , dynamic viscosity μ , heat capacity ratio γ , thermal conductivity κ , heat capacity at constant pressure c_p , binary mass diffusion coefficient D , and thermal diffusivity K_T —all must be evaluated for a binary mixture. For atomic gases, $\gamma = 1.667$ at room temperature. The density ρ_0 and heat capacity at constant pressure c_p were computed through simple mole fraction relations:

$$\rho = x\rho_{\text{Ar}} + (1 - x)\rho_{\text{He}} \quad (6)$$

and:

$$c_p = xc_{p,\text{Ar}} + (1 - x)c_{p,\text{He}} \quad (7)$$

where x is the mole fraction of Ar and, implicitly, $(1-x)$ is the mole fraction of He. The mixture transport coefficients μ , κ , D , and K_T can be calculated from kinetic theory using the Lennard–Jones potential as a molecular model (Hirschfelder et al. 1964). The force constants of the mixture for this potential were obtained from the force constants of the pure species using the Lorentz–Bertholet combining rules:

$$r = \frac{r_{\text{He}} + r_{\text{Ar}}}{2} \quad \text{and} \quad \frac{\epsilon}{k} = \sqrt{\frac{\epsilon_1 \epsilon_2}{k_1 k_2}} \quad (8)$$

where r is the collision diameter, and ϵ/k is the potential parameter.

2 Experimental

The optical setup for the TGS experiments is shown schematically in Fig. 1. The frequency-doubled output of a Q-switched Nd:YAG laser was used to generate the

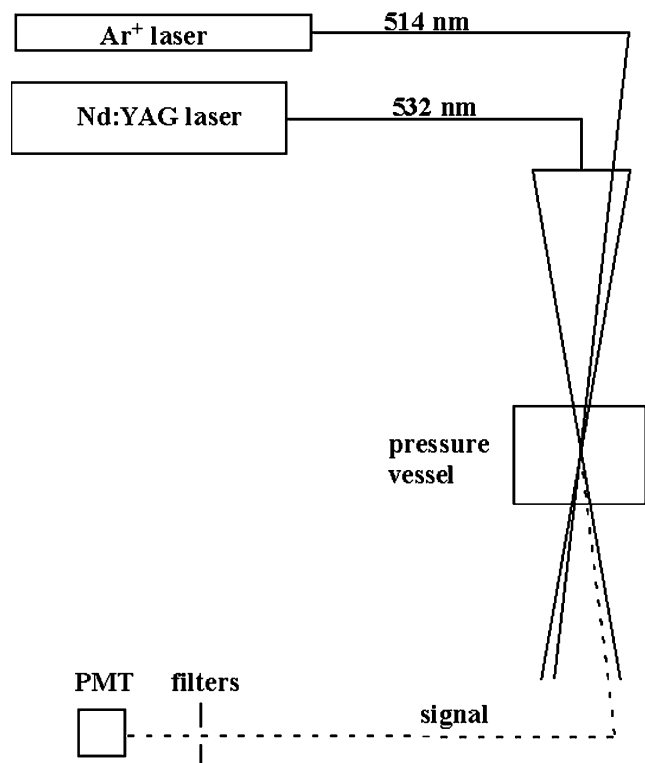


Fig. 1 Schematic of the transient-grating spectroscopy (TGS) optical setup. The beam-crossing angle is typically on the order of a few degrees and is greatly exaggerated in this schematic. During alignment, 4% of the probe beam was used to trace the path of the signal beam

gratings. This short pulse beam (~ 10 ns) was divided into two pump beams of equal energy using a 50/50 beam splitter. The pump energy was varied from 10 mJ to 150 mJ per pulse for both beams. The 514-nm output (~ 1 W) of an Ar-ion laser was used as the probe beam for reading out the gratings. For tracing out the path of the generated TGS signal beam, $\sim 4\%$ of the probe beam was split off and steered through the probe volume at the Bragg angle. This false signal beam was used during the alignment of the detector and eliminated during the actual experiments. The three (or four when the false signal was included) laser beams were directed into the sample volume inside the high-pressure gas cell with a three-dimensional phase-matching arrangement. The signal beam was directed by a mirror through spatial and spectral filters and onto a photomultiplier tube (PMT). The PMT was connected to a digital oscilloscope for acquiring the TGS signals. The signals were typically acquired and stored in a computer for subsequent off-line analysis. The 12.7-cm-diameter high-pressure gas cell was designed to operate at pressures of up to 35 atm. To provide optical access, two 25.4-mm-thick BK-7 windows were mounted along the optical path. Measurements were made at room temperature over a range of pressures extending from 1 atm to 7.4 atm.

When the probe volume diameter is small (as with focused pump beams), the effect of the sound waves

propagating out of the probe volume makes a significant contribution to the apparent grating decay rate. Therefore, it is more difficult to extract accurately the acoustic damping rate from TGS signals generated using focused laser beams where the probe volume is typically a few hundred microns in diameter at the waist and the TGS signals decays to zero after a few hundred nanoseconds. For measurements in reacting flows—where high temperatures result in low density and, hence, low signal levels—focused beams are required for the generation of detectable signals. In the present TGS experiments, unfocused laser beams were used to investigate the acoustic damping rates. The diameter of the probe volume is ~ 8 mm, resulting in TGS signals that persist for up to a few microseconds. The lowest acoustic damping rates were measured in pure argon and were equal to 20×10^{-6} m²/s at 1 atm. For our grating spacing of 22.4 μ m, this yields a decay time of 0.64 μ s. At these same conditions, the acoustic wave walkout time for 8-mm beams is ~ 25 μ s. Hence, the measured damping rates need not be corrected for finite beam size effects. Because these measurements were made at room temperature, the pump intensity provided by unfocused beams was sufficient to generate high signal strengths (recall that signal strength scales quadratically with density). When high spatial resolution is required, as in inhomogeneous environments, focused pump beams should be used and attention should be paid to the effect of sound wave propagation out of the probe volume. A comparison of sample TGS signals generated by focused and unfocused pump beams is shown in Fig. 2.

During the experiments, Ar and He were introduced into the high-pressure chamber separately. The TGS signals were acquired when the macroscopic flow field motions were completely dissipated and the gases well mixed. The generation of an electrostrictive grating in He is very difficult, especially with unfocused pump beams, because of the very low electrostriction coefficient of helium. To generate a detectable signal, a small amount of NO₂ (< 100 ppm) was seeded into the gas samples to generate resonant TGS signals through the thermalization process. An optically resonant trace seed gas for signal generation is routinely used in transient-grating measurements (Cummings et al. 1995; Schlamp et al. 2000; Schlamp and Sobota 2002). The seed gas absorbs energy from the pump laser beams through an allowed electronic resonance. Inelastic collisions transfer the electronic energy to translation energy, locally heating the gas, and leading to the desired grating formation (Paul et al. 1995). The energy transfer typically occurs on time scales that are orders of magnitude smaller than the acoustic time scale; hence, thermalization has no direct impact on the temporal structure of the TGS signal. The temperature perturbation of the thermalization process, $\Delta T/T$, is on the order of 10^{-4} to 10^{-5} ; thus, the mean thermophysical state of the target fluid is not changed. The 532-nm pump beams used in this study overlap with a broad NO₂ absorption band arising from a low-lying electronic state (Okabe 1978).

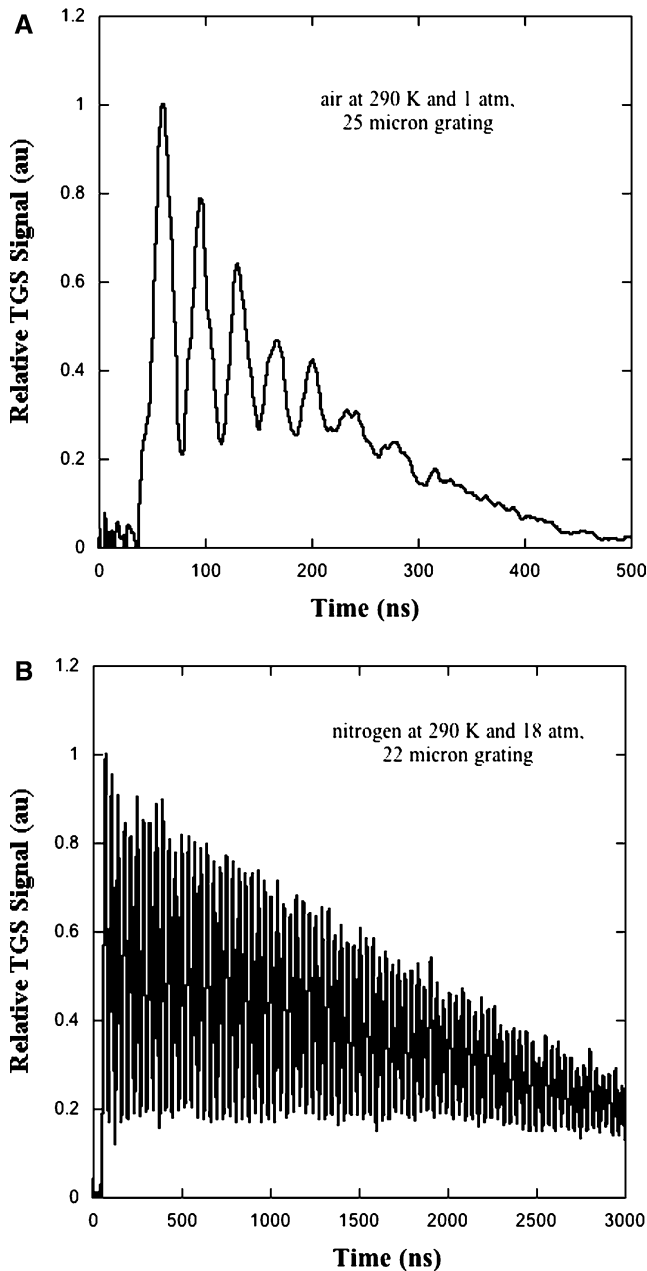


Fig. 2a, b Relative TGS signals from air at STP, generated with focused beams (a) and TGS signals from nitrogen at 18-atm pressure, generated with unfocused beams (b). The TGS signals were generated via electrostriction in both cases. The probe volume diameter was 200 μm for the focused beam geometry and 8 mm for the unfocused beam geometry. Grating spacing is similar in both examples and was 64-shot average. Note the differences in the time scales

The mole fractions of Ar and He in the mixtures employed in this study were calculated by analyzing the oscillation frequencies of the TGS signals. From an analysis presented elsewhere (Brown and Roberts 1999), a relationship exists between the temperature and frequency of the TGS signal generated through the thermalization process:

$$T = f^2 \Lambda^2 \left(\frac{M}{\gamma} \right) \frac{1}{R} \quad (9)$$

In a binary mixture of Ar with mole fraction x and He with mole fraction $(1-x)$, the molecular weight of the mixture is:

$$M = xM_{\text{Ar}} + (1-x)M_{\text{He}} \quad (10)$$

where M_{Ar} and M_{He} are the molecular weights of Ar and He, respectively. If Eqs. 9 and 10 are combined, the mole fraction of Ar in an He–Ar mixture can be accurately calculated by measuring the TGS signal frequency:

$$x = \frac{\gamma RT - M_{\text{He}} \Lambda^2 f^2}{(M_{\text{Ar}} - M_{\text{He}}) \Lambda^2 f^2} \quad (11)$$

In Eq. 11, the temperature T is known (room temperature) and the grating spacing Λ can be determined from calibration using TGS signals from a single species (Ar, in this case). Therefore, the mole fractions of Ar and He can be easily evaluated by analyzing the oscillation frequency f of the acquired TGS signals.

3 Results and discussion

The acoustic damping rates of He–Ar mixtures under various pressures and mole fractions were investigated. All signals analyzed in the present study are due to the resonant optical response of the seeded NO_2 . The acoustic wave frequency ranges from ~ 14 MHz in pure argon to ~ 45 MHz in pure helium at a grating spacing of 22.4 μm . In this frequency–pressure region, dispersion of the acoustic absorption rate is negligible (Prangma et al. 1970). The acoustic damping rate is extracted by curve fitting the TGS signal with Eq. 2. In this equation, A , B , D_{th} , C_s , and Γ were used as the fitting parameters. Thermal diffusivity, D_{th} , can be extracted during curve fitting. However, since $A \exp(-D_{\text{th}} q^2 t)$ represents the DC component, which is only a small contribution to the overall signal in these gas mixtures, the accuracy is low and we do not report values of D_{th} here. Accurate values of D_{th} can, and have been, reported in the literature for other gas mixtures. Commercial software (KaleidaGraph) that employs the Levenberg–Marquardt algorithm was utilized in the nonlinear least-squares fit of the TGS signals. A sample of a TGS signal and the curve fitting result are shown in Fig. 3. The curve fitting error is usually less than 5%, as described elsewhere (Li et al. 2002).

Since the factor $1/\rho_0$ in Eq. 4 and the mass diffusion coefficient D in Eq. 5 are both proportional to the inverse of the pressure, while other transport properties, such as viscosity μ , thermal conductivity κ , and thermal diffusivity K_T , are not significant functions of pressure (Hirschfelder et al. 1964), the total acoustic damping rate, Γ , will scale with the inverse of pressure. Therefore, the reduced acoustic damping rate given by the product

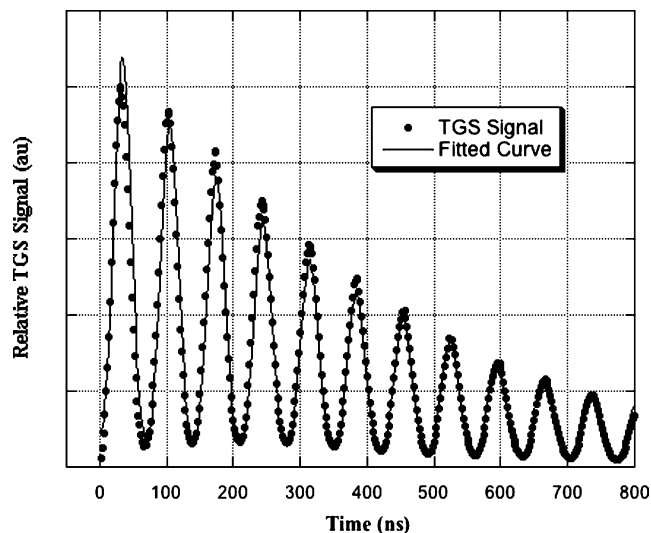


Fig. 3 The TGS signal in pure argon with curve fitting. Pressure = 1.0 atm, pump energy = 105 mJ/pulse, probe power = 0.6 W, grating spacing $\Lambda = 22.4 \mu\text{m}$, and 64-shot average. The acoustic damping rate derived from curve fitting is $1.68 \times 10^{-5} \text{ m}^2/\text{s}$, while theoretical calculations yield $1.44 \times 10^{-5} \text{ m}^2/\text{s}$

of the acoustic damping rate and the pressure, Γp , is independent of pressure. Figure 4 shows the experimental and both classical and modified theoretical values of the reduced acoustic damping rate from the He–Ar mixtures at 1, 2.4, 4.1, and 7.4 atm. The experimental data was 64-shot averaged, with an expected accuracy of 12% (taking into account the 5% accuracy of the curve fitting mentioned above). The error bars shown in Fig. 4 on the 2.4-atm data reflect this degree of uncertainty.

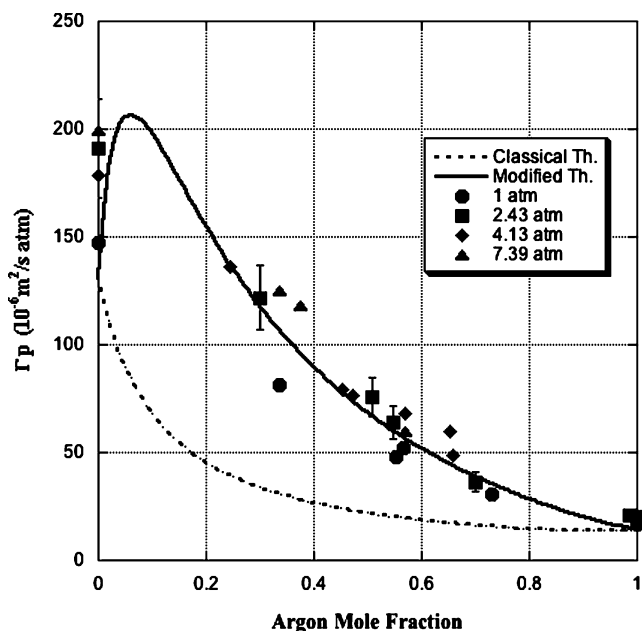


Fig. 4 Comparison of experimental and theoretically [both visco-thermal (classical) and modified to include mass diffusion (Kohler's theory)] predicted results for the acoustic damping rate in He–Ar mixtures at 1, 2.43, 4.13, and 7.39 atm. Grating spacing $\Lambda = 22.4 \mu\text{m}$

The theoretical values were calculated using $\Gamma_c p$ for the classical theory and $\Gamma p = (\Gamma_c + \Gamma_d)p$ for the modified theory. Overall, the experimental results display good agreement with theory and show the trend of Γp changing with species concentration.

The addition of a very small amount of impurity gas into a pure sample or gas mixture will alter the sound speed and other intrinsic properties, such as the compressibility, to a degree that is commensurate with the mole fraction of the impurity. However, the collisional relaxation time of the total mixture may be altered in a disproportionate manner with respect to the mole fraction of the impurity (Zuckerwar 2002). This is particularly true when a trace amount of a molecular gas is added to an atomic gas. The ro-vibrational states of the molecular species are coupled to the translational states through collisions and provide another means for damping out the density perturbations. The disproportionate influence on relaxation is dependent on the host gas and is strongest for He (Zuckerwar 2002). As a result of relaxation, the acoustic damping coefficient is modified by a term that scales as the inverse of the product of c_s , q , and τ_a , where τ_a denotes the collisional relaxation time of the molecular species (Zuckerwar 2002). This additional term is often folded into the bulk viscosity for computational convenience (Berne and Pecora 1990). Acoustic attenuation is increased in the atomic gas with the addition of the trace molecular species. In short, the addition of a trace molecular species, such as NO_2 , to He will increase the acoustic damping beyond that expected for pure He, and the effect will be in excess of the mole fraction of the trace species. In the experiments described here, gases were introduced into the test cell sequentially, and partial pressures were used, in part, to assess mixture fractions. The TGS sound speed measurement was also used for accurate assessment of the relative amounts of Ar and He. While the mole fraction of NO_2 was held below 100 ppm, the exact value for each measurement shown in Fig. 4 is unknown. In effect, some small uncertainty exists in the calculated bulk viscosity and, consequently, in the acoustic damping coefficient. This uncertainty is reflected in the difference between the calculated and the measured damping coefficient at low Ar concentrations. As expected from the above considerations, the observed acoustic damping is larger than that calculated for 0% Ar addition. Also, the small amount of scatter in the data for all Ar concentrations is due, in part, to relative differences in the amount of NO_2 present.

4 Summary

It has been demonstrated that transient-grating spectroscopy (TGS) can be used to measure acoustic damping coefficients in gas mixtures without the need for extended propagation distances. TGS measurements can be made in small volumes and in harsh environments that are not amenable to acoustic transducer/re-

ceiver setups. It has also been demonstrated that TGS is capable of single-shot measurements (Brown et al. 2003), rendering the technique nearly instantaneous (on the order of a few hundred nanoseconds), as compared to most other reacting flow field time scales. The potential to measure acoustic damping rates in inhomogeneous and unsteady flows makes TGS an attractive alternative to traditional measurement techniques. This study indicates the role of mass diffusion in determining acoustic damping when the local density field in a fluid is optically perturbed. Consistent with previous studies, it also indicates the strong influence of a trace molecular species on acoustic damping in an atomic host.

References

- Berne BJ, Pecora R (1990) Dynamic light scattering, Chap 10. Krieger Publishing, Malabar, Florida
- Brown MS, Roberts WL (1999) Single-point thermometry in high-pressure, sooting, premixed combustion environments. *J Prop Power* 15:119–127
- Brown MS, Li Y, Roberts WL, Gord JR (2003) Analysis of transient grating signals for reacting flow applications. *Appl Opt* 42:566–578
- Cummings EB, Leyva IA, Hornung HG (1995) Laser-induced thermal acoustics (LITA) signals from finite beams. *Appl Opt* 34:3290–3302
- Eichler HJ, Gunter P, Pohl DW (1986) Laser-induced dynamic gratings. Springer, Berlin Heidelberg New York
- Govoni DE, Booze JA, Sinha A, Crim FF (1993) The non-resonant signal in laser-induced grating spectroscopy of gases. *Chem Phys Lett* 216:525–529
- Herzfeld KF, Litovitz TA (1959) Absorption and dispersion of ultrasonic waves. Academic Press, New York
- Hirschfelder JO, Curtiss CF, Bird RB (1964) Molecular theory of gases and liquids, Chap 8. Wiley, New York
- Holmes R, Tempest W (1960) The propagation of sound in monoatomic gas mixtures. *Proc Phys Soc (Lond)* 75:898–904
- Kohler M (1941) Die volumviskosität in idealen gasen als gaskinetische transporterscheinung. *Ann Physik* 39:209–225
- Kohler M (1949) Schallabsorption in binaren gasmischungen. *Ann Physik* 127:41–48
- Law AK, Koronaios N, Lindsay RB (1966) Effect of diffusion on ultrasonic attenuation in mixtures of rare gases. *J Acoust Soc Am* 41:93–99
- Li Y, Roberts WL, Brown MS (2002) Investigation of gaseous acoustic damping rates by transient grating spectroscopy. *AIAA J* 40:1071–1077
- Okabe H (1978) Photochemistry of small molecules. Wiley, New York
- Paul PH, Farrow RL, Danehy PM (1995) Gas-phase thermal-grating contributions to four-wave mixing. *J Opt Soc Am B* 12:384–392
- Prangma GJ, Jonkman RM, Beenakker JJM (1970) Sound-absorption measurements in helium-argon mixtures in the “Burnett region.” *Physica* 48:323–330
- Schlamp S, Sobota TH (2002) Measuring concentrations with laser-induced thermalization and electrostriction gratings. *Exp Fluids* 32:683–688
- Schlamp S, Cummings EB, Sobota TH (2000) Laser-induced thermal-acoustic velocimetry with heterodyne detection. *Opt Lett* 25:224–226
- Trusler JPM (1991) Physical acoustics and metrology of fluids. Hilger, Bristol, UK
- Zuckerwar AJ (2002) Handbook of the speed of sound in real gases, Chap 5. Academic Press, Amsterdam, The Netherlands